

HARD: A Performance Portable Radiation Hydrodynamics Code based on FLECSI Framework

Julien Loiseau^a, Hyun Lim^a, Andrés Yagüe López^a, Mammadbaghir Baghirzade^b, Shihab Shahriar Khan^c, Yoonsoo Kim^d, Sudarshan Neopane^e, Alexander Strack^f, Farhana Taiyebah^g, Ben Bergen^a

^a*Los Alamos National Laboratory*

^b*The University of Texas at Austin*

^c*Michigan State University*

^d*Princeton Center for Theoretical Science*

^e*University of Tennessee, Knoxville*

^f*Universität Stuttgart*

^g*Florida State University*

Abstract

Hydrodynamics And Radiation Diffusion (HARD) is an open-source application for high-performance simulations of compressible hydrodynamics with radiation-diffusion coupling. Built on the FLECSI [1] (Flexible Computational Science Infrastructure) framework, HARD expresses its computational units as tasks whose execution can be orchestrated by multiple back-end runtimes, including Legion [2], MPI [3], and HPX [4]. Node-level parallelism is delegated to Kokkos [5], providing a single, portable code base that runs efficiently on laptops, small homogeneous clusters, and the largest heterogeneous supercomputers currently available.

To ensure scientific reliability, HARD includes a regression-test suite that automatically reproduces canonical verification problems such as the Sod and LeBlanc shock tubes, and the Sedov blast wave, comparing numerical solutions against known analytical results. The project is distributed under an OSI-approved license, hosted on GitHub, and accompanied by reproducible build scripts and continuous integration workflows. This combination of performance portability, verification infrastructure, and community-focused development makes HARD a sustainable platform for advancing radiation hydrodynamics research across multiple domains.

Keywords: Task Based Parallelism, Hydrodynamics, Radiative Diffusion

Nr.	Code metadata description	Metadata
C1	Current code version	V1.0
C2	Permanent link to code/repository used for this code version	https://github.com/lanl/hard
C3	Permanent link to Reproducible Capsule	
C4	Legal Code License	BSD 3-Clause License
C5	Code versioning system used	git
C6	Software code languages, tools, and services used	C++, MPI
C7	Compilation requirements, operating environments & dependencies	Kokkos, Singularity-EOS
C8	If available Link to developer documentation/manual	https://lanl.github.io/HARD/
C9	Support email for questions	hard-help@lanl.gov

Table 1: Code metadata (mandatory)

Metadata

1. Motivation and significance

Radiation hydrodynamics (RHD) governs systems where radiation–matter coupling shapes the global dynamics, including high-energy-density physics (HEDP) problems such as inertial confinement fusion (ICF), stellar evolution and explosions, accretion flows, and radiative shocks. Accurately capturing these phenomena requires solving tightly coupled, nonlinear partial differential equations for hydrodynamics and radiation diffusion across disparate spatial and temporal scales, often in the presence of stiff source terms and strong gradients.

While several mature RHD and radiation–Magnetohydrodynamics (MHD) codes exist [6, 7, 8, 9, 10, 11], many legacy implementations face practical challenges on modern heterogeneous platforms such as limited performance portability, rigid data models that impede algorithmic experimentation, and difficulty integrating with contemporary tooling for CI, packaging, and reproducibility. As experimental capabilities and computing architectures evolve, a software platform that cleanly separates physics from execution back ends, and that scales from laptops to leadership-class systems, becomes essential. HARD is designed to meet this need. Built on the task-based FLECSI runtime layer, it decouples application physics from parallel orchestration. This design enables the same source to target multiple distributed-memory runtimes (Legion, MPI, and HPX) while delegating node-level parallelism to

Kokkos through an abstraction layer, yielding a single, portable implementation for CPUs and GPUs. Beyond portability, HARD aims to serve as a *testbed* for new methods in RHD by providing clear interfaces for numerics (reconstruction, Riemann solvers, time integrators) and physics (equations of state, radiation closures).

To promote scientific reliability and re-use, HARD includes:

- a regression test suite that automatically reproduces canonical verification problems (e.g., Sod and LeBlanc shock tubes, Sedov blast) and compares against analytic or reference solutions;
- containerized and scriptable builds to ensure bitwise-reproducible environments across developer machines and CI;
- open-source governance and contribution workflows to lower the barrier for community extensions (e.g., MHD, multigroup radiation, advanced microphysics).

In summary, HARD addresses two complementary gaps: (i) a performance-portable RHD code that maps cleanly to heterogeneous architectures, and (ii) a modular, reproducible platform that accelerates method development and cross-code comparison for the RHD community.

2. Software description

HARD is implemented in modern C++ for UNIX and high-performance computing (HPC) platforms, taking advantage of the Standard Template Library (STL). Spack [12] is used to configure both build- and run-time environments. Simulation data is written in CSV and Catalyst formats, enabling post-processing with visualization tools such as ParaView [13] and VisIt [14].

2.1. Software architecture

The software stack is shown in Figure 1. HARD uses a FLECSI specialization layer that employs the N-Array topology (a multidimensional array with exclusive, shared, and ghost entities).

The HARD base code defines its specialization in `spec/`, and the application that uses the specialization in `app/`. The current control model consists of initialization, time-stepping (advection, diffusion, and source updates), and output.

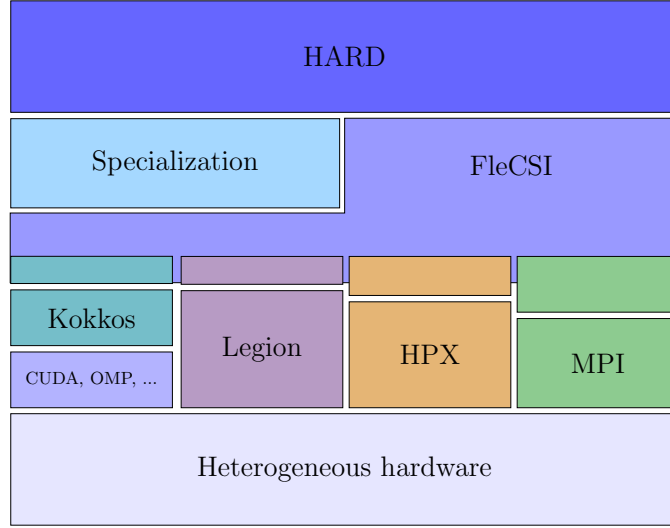


Figure 1: HARD within the FLECSI ecosystem.

2.2. Software functionalities

HARD provides a set of core capabilities for solving RHD problems on modern HPC systems. At a high level, these include:

- implementation of the coupled hydrodynamics and radiation–diffusion equations,
- modular numerical algorithms (finite-volume solvers, reconstruction methods, Riemann solvers, and implicit diffusion solvers),
- verification problems and regression tests for scientific reliability, and
- scalable distributed parallel execution across CPUs and GPUs via FLECSI back ends.

The following subsections describe the mathematical models, numerical algorithms, and example problems that illustrate these capabilities.

2.2.1. Basic Equations

We adopt the co-moving (Eulerian) frame formulation of the RHD equations in the diffusion limit [15]. This formulation is particularly well-suited for regimes where the mean free path of photons is small compared to the characteristic hydrodynamic length scales, allowing the radiative flux to be

described by a diffusion approximation. In this framework, the governing equations can be compactly expressed in Einstein notation as

$$\partial_t \mathbf{U} + \partial_j \mathbf{F}^j = \mathbf{S} \quad (1)$$

with the evolved variables

$$\mathbf{U} = [\rho, \rho v^i, e + \rho v^2/2, E]^T, \quad (2)$$

fluxes

$$\mathbf{F}^j = \begin{bmatrix} \rho v^j \\ \rho v^i v^j + p \delta_{ij} \\ (e + \rho v^2/2 + p) v^j \\ E v^j \end{bmatrix}, \quad (3)$$

and source terms

$$\mathbf{S} = \begin{bmatrix} 0 \\ f^i \\ f^i v_i + \dot{q} \\ -\partial_i F_r^i - P_r^{ij} \nabla_i v_j - \dot{q} \end{bmatrix}, \quad (4)$$

where ρ is fluid mass density, v^i is the component i of the fluid velocity vector, e is the fluid internal energy density, p is the fluid pressure, E is radiation energy density, F_r^i is the component i of the radiation energy flux vector, P_r^{ij} is the i, j element of the radiation pressure tensor, f^i is the component i of the radiation force density vector

$$f^i = \frac{\kappa \rho}{c} F_r^i, \quad (5)$$

and \dot{q} is the radiative heating rate

$$\dot{q} = \frac{dq}{dt} = c \kappa \rho (E - a T^4), \quad (6)$$

where κ is the mean opacity, c is the speed of light, T is the fluid temperature, and a is the radiation defined as $a \equiv 4\sigma/c$, where σ is the Stefan-Boltzmann constant.

To close the evolution system for the fluid, it is necessary to specify the functional form of the fluid pressure p , which can be obtained from an equation of state (EoS). In this work, we adopt **Singularity-EoS** [16], which provides a flexible EoS framework that enables the modeling of different materials. The radiative transfer equation—the final component of the evolution system given in Equation 1—further requires closure relations for both the radiation energy flux density F^i and the radiation pressure tensor P_r^{ij} .

In the optically-thick diffusion limit, they are given as

$$F^i = -\frac{c}{3\kappa\rho}\nabla E, \quad (7)$$

$$P_r^{ij} = \frac{1}{3}E\delta_{ij}, \quad (8)$$

provided the mean free path of photons are much shorter than the length scale of interest.

The evolution equations presented above are valid in the diffusion (optically thick) limit. However, it is possible to extend their applicability to optically thin regimes by introducing a bridge law [6], which ensures that the radiation energy flux density F_r^i attains the correct magnitude in the free-streaming limit.

$$F_r^i = -\lambda\frac{c}{\kappa\rho}\nabla E \quad (9)$$

Here, λ is a radiation energy flux limiter function [17]

$$\lambda = \frac{2 + R}{6 + 3R + R^2} \quad (10)$$

$$R \equiv \frac{|\nabla E|}{\rho\kappa E} \quad (11)$$

$$\frac{P^{ij}}{E} = \left(\frac{1-f}{2}\right)\delta_{ij} + \left(\frac{3f-1}{2}\right)n^i n^j \quad (12)$$

where $n^i \equiv \nabla E/|\nabla E|$ and the quantity f is defined as

$$f = \lambda + \lambda^2 R^2. \quad (13)$$

In the optically thick limit, where $R \rightarrow 0$, one finds $\lambda \rightarrow 1/3$ and $f \rightarrow 1/3$, such that the Eddington approximation, $P^{ij} = (E/3)\delta_{ij}$, is recovered. In contrast, in the optically thin limit, the photon field streams along the gradient of the local radiation energy density at the speed of light. Although these prescriptions do not constitute a fully self-consistent treatment of light-matter interactions, they provide a computationally efficient closure that smoothly bridges the optically thick and thin regimes. As a result, the radiative transfer equation becomes

$$\partial_t E + \partial_j(Ev^j) = \partial_i(D\partial_i E) - P_r^{ij}\nabla_i v_j - \dot{q}, \quad (14)$$

with $D = c\lambda/\kappa\rho$.

2.2.2. Numerical algorithms

The computational domain is represented by a uniform Cartesian mesh, with evolved variables located at the center of each cell. In this section, we abandon Einstein notation and limit our notation to a single dimension for clarity. We use an operator split approach to handle the conservative advection equations (3) and the non-advective part of the radiation transfer equations (14). The advection parts are solved using a finite volume method, with the discretization

$$\frac{\partial F_x}{\partial x} \rightarrow \frac{F_{x_{i+1/2}}^* - F_{x_{i-1/2}}^*}{\Delta x_i} \quad (15)$$

where $F_{x_{i\pm 1/2}}^*$ are the numerical fluxes computed at each of the cell faces $x_{i\pm 1/2}$ around cell coordinate x_i in meshpoint i , and are obtained with an approximate Riemann solver along with an appropriate face reconstruction heuristic from cell-centered values. We employ the WENO5-Z reconstruction [18] for all variables, where we adopt the HLL fluxes [19] for hydrodynamics variables and the local Lax-Friedrichs (Rusanov) fluxes [20] for the radiation energy density. The time advance is done using Heun's method for a second-order approximation in time. A Butcher tableau is given in Table 2.

0		
1	1	
<hr/>		
	1/2	1/2

Table 2: Butcher tableau for Heun's method (second-order RK).

The diffusive part of the radiative transfer equations is solved with a geometric multigrid solver (GMG) with regular coarsening. GMG solves the elliptic equation

$$Au = f, \quad (16)$$

where A is a linear operator. Multigrid solvers use successively coarser grid representations of the simulation domain to accelerate convergence by a recursion that combines the ability of elementary iterative solvers to damp high-frequency errors with coarse-grid error corrections. On each coarse grid level, elementary iterative solvers are again effective at damping high-frequency error until some reduced set of unknowns can be solved directly. The resulting error corrections are prolonged to the next finer grid with some small number of smoothing cycles applied to eliminate noise. Using this technique appropriately results in asymptotically optimal convergence, i.e., $O(n)$ for n unknowns [21, 22].

For every grid except for the so-called “solution grid” (i.e., the finest grid), the equation being solved is the residual of Equation (16),

$$r = f - Au' \implies Ae = r, \quad (17)$$

with $e = u_c - u'$ where u_c is a better approximation to the solution u given by the previous approximation u' . The advantage of the residual is that a good initial guess is well known as $r_0 = 0$. The error field e is then transported to the finer grid to correct the previous approximation to the solution u' in that level. Equation (17) is only correct if

$$Ae = r \implies A(u_c - u') = f - Au' \implies Au_c = f, \quad (18)$$

which necessitates that A is a linear operator.

The coarsest level in this progression ideally has many fewer nodes than the solution grid allowing for computationally expensive but more accurate methods, such as the Conjugate Gradient method. In our current implementation of the code a simple relaxation method is used instead. In the future, we will use linear solvers from the parallel solver library `FleCSolve` [23] for this step.

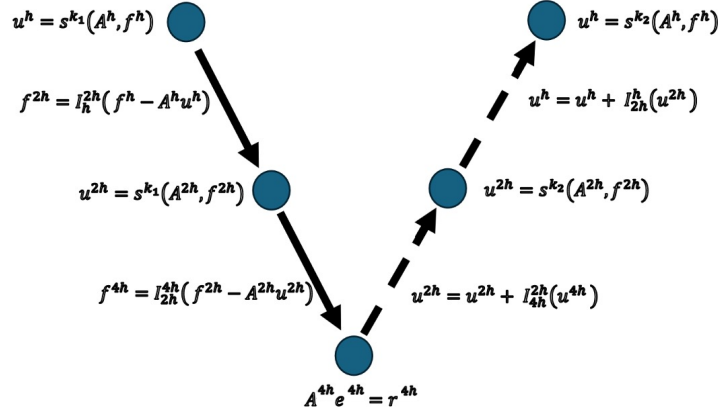


Figure 2: A v-cycle, the most basic structure of a GMG solver. Every circle represents a different grid level, with circles higher up representing finer grids where h is the distance between two consecutive nodes in the grid. The restriction and prolongation operations are represented with the I operator, and the relaxation solver applied k times is represented with the s^k operator. The specific notation used in this figure can be found in any of the references provided for GMG.

The most basic structure of a GMG solver is known as a v-cycle, illustrated in figure 2.

3. Illustrative examples

In this section, we provide several cases to demonstrate validation and functionalities of the code. The problems used to test the code fall into three categories. First, we demonstrate with hydrodynamics problem, then we isolate the heating and cooling term, and finally show the full RHD test problems.

For the following tests, we will quantify the error between the numerical and analytical solutions with the L_1 metric defined as

$$L_1 = \Delta V \sum |N_i - \langle A(x_i) \rangle|, \quad (19)$$

where N_i is the numerical solution at grid coordinate x_i , $\langle A(x_i) \rangle$ is the volume-averaged analytical solution over the finite volume containing element i , and ΔV is the volume element of the regular grid. $\langle A(x_i) \rangle$ is calculated using a Gauss-Legendre quadrature with 10 nodes.

3.1. Basic hydrodynamics problem: Sod shock tube test

The Sod shock tube is a standard Riemann problem test with the following initial parameters:

$$(\rho, v, p)_{t=0} = \begin{cases} (1.0, 0.0, 1.0) & \text{if } 0.0 < x \leq 0.5, \\ (0.125, 0.0, 0.1) & \text{if } 0.5 < x < 1.0. \end{cases} \quad (20)$$

This leads to the development of a shock front, which propagates from high-density into low-density regions, followed by a contact discontinuity, while a rarefaction wave propagates.

The numerical and analytical solution comparison for density in the Sod tube in HARD is shown in Figure 3.

3.2. Radiation test problem: heating and cooling

We perform a standard heating and cooling of the fluid by radiation [24]. The mass density of the fluid is set to $\rho = 10^{-7} \text{ g cm}^{-3}$, with a mean molecular weight of $\mu = 0.6$ and an opacity of $\kappa = 0.4 \text{ cm}^2 \text{ g}^{-1}$. A uniform radiation field is initialized with a temperature of $T_{0,r} = 3.4 \times 10^6 \text{ K}$. In this test, we consider two scenarios: the fluid is heated by radiation; and the fluid cools. For the heating case, the fluid is initialized at $T_{0,f,\text{heating}} = 11 \text{ K}$, while for the cooling case the initial temperature is $T_{0,f,\text{cooling}} = 1.1 \times 10^9 \text{ K}$. In both scenarios, the radiation energy density exceeds the internal energy of the fluid and, thus, remains nearly constant during the energy exchange. Consequently, the fluid eventually equilibrates to the radiation temperature.

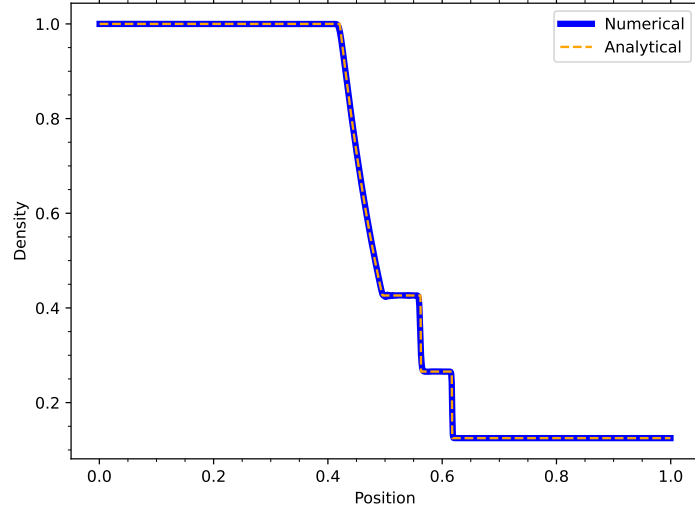


Figure 3: Numerical and analytical solution to the Sod problem at simulation time $t = 0.0669$ with $dx = 2^{-10}$ and $dt = 0.3$ CFL. The L_1 error for this figure is below $5 \cdot 10^{-4}$.

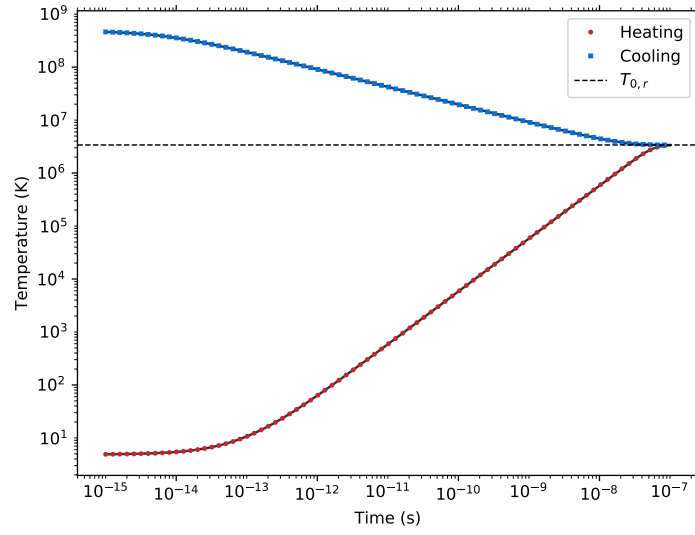


Figure 4: Tests of the approach to radiative equilibrium in a radiation dominated gas. Both cases approach the equilibrium value and matches with the analytical solution (solid lines).

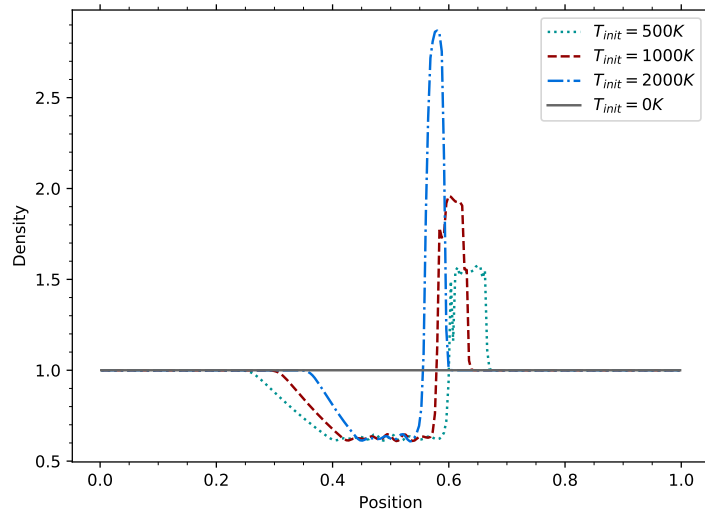


Figure 5: The Temperature induced shock test problem with different initial temperatures at $t = 0.5$. The radiation temperature is the only driving source, so $T = 0$ K shows no shock formation. In contrast, nonzero- T cases exhibit shock formation.

An analytic benchmark solution can be obtained by solving the ODE in Equation (6).

Figure 4 presents the numerical results of the heating-cooling test alongside a reference solution (solid lines) obtained by integrating Equation (6) with an ODE solver. The numerical solutions show agreement with the reference results and asymptotically converge to the radiation temperature, as expected.

3.3. Radiation hydrodynamics problem: temperature induced shock

In scenarios such as ICF, where energy from laser or X-ray drivers rapidly heats a thin outer layer of a fusion capsule, thermal energy deposition creates steep pressure gradients that launch shock waves. In these systems, radiation diffusion plays a critical role by preheating material ahead of the shock front, altering the shock structure and modifying compression and temperature profiles. To test this phenomenon, we perform temperature-induced shock problems in 1D [25]. Figure 5 shows a temperature-induced shock test problem that is examined at time $t = 0.5$ for different initial temperatures. We apply an ideal EoS for this test problem. Since radiation temperature is the sole driving mechanism, the case with $T = 0K$ does not exhibit shock formation. In contrast, cases with nonzero initial temperatures demonstrate the development of shock structures. This test provides a simplified yet powerful framework to benchmark simulation codes, explore radiation-matter

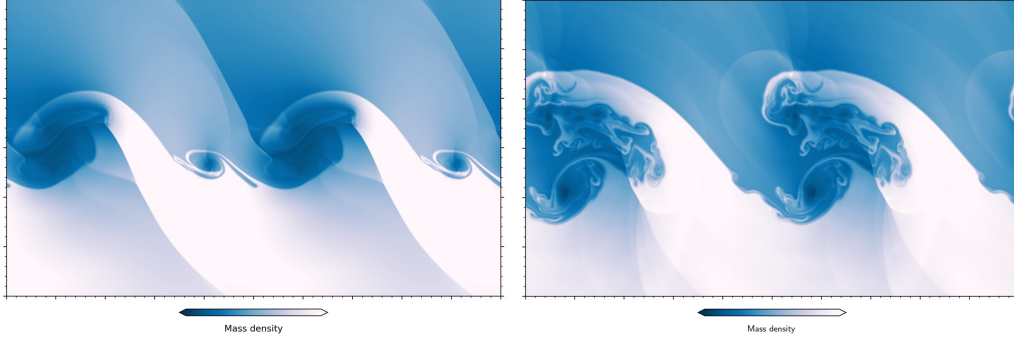


Figure 6: Density plot of Kelvin-Helmholtz instability with (right) and without (left) radiation at $t = 16s$. The radiation case shows the instability is destabilizing with the presence of radiation field.

coupling, and study shock timing and strength, all essential for optimizing performance in ICF experiments.

3.4. Radiation hydrodynamics problem: radiative Kelvin-Helmholtz instability

The Kelvin-Helmholtz instability (KHI) is a fundamental shear-flow instability that arises when there is velocity shear within a continuous fluid or across the interface between two fluids moving at different speeds [26]. KHI is important to understand various phenomena, from shear layers in accretion flows and at stellar surfaces to laboratory experiments relevant to inertial confinement fusion.

Linear analyses [27, 28] show that the presence of a radiation field increases the growth rates of unstable modes, thereby shortening the characteristic instability timescale. Motivated by this result, we perform two-dimensional simulations of KHI with and without radiation. The computational domain is the square $\{(x, y) \mid -0.5 \leq x \leq 0.5, -0.5 \leq y \leq 0.5\}$. We initialize two layers of different density, $\rho_{\text{low}} = 1.0$ and $\rho_{\text{high}} = 2.5$, and prescribe a piecewise-constant streamwise velocity: $v_x = -0.5$ for $|y| \leq 0.25$ and $v_x = 0.5$ elsewhere. In the radiative case, a spatially uniform radiation temperature $T_{\text{rad}} = 1000 \text{ K}$ is imposed throughout the domain.

Figure 6 shows the density field at $t = 16s$ for the radiative (right) and non-radiative (left) runs. Consistent with linear theory, radiation accelerates the development of KHI, leading to faster growth of instabilities. A systematic exploration of parameter dependence and radiative effects will be reported in future work.

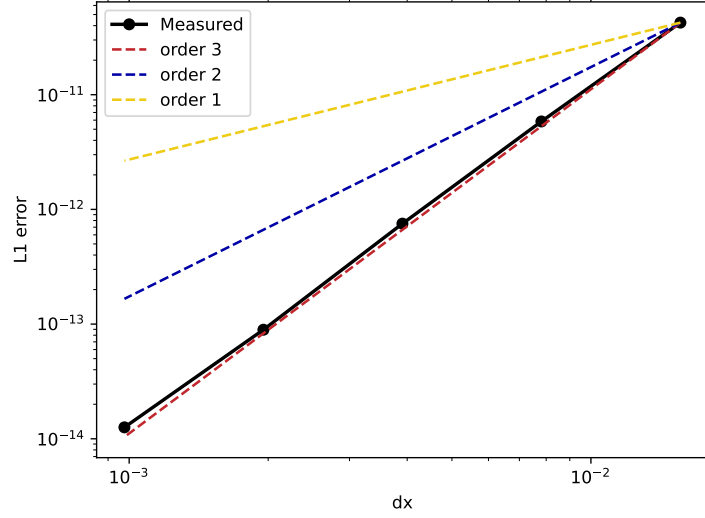


Figure 7: Convergence order for an acoustic wave problem with weno5z as limiter

3.5. Numerical Convergence

To study the convergence of the code, see Figure 7, where we run an acoustic wave problem with a WENO5-Z limiter [6]. We choose the same final time for subsequent, smaller grids, with a timestep given by the Courant–Friedrichs–Lewy (CFL) condition.

The acoustic wave problem can be understood by linearizing Equation (1), defining each primitive field as a homogeneous equilibrium value and a *small* perturbation. Assuming the perturbation shape can be decomposed in Fourier modes, it is enough to apply the linearized equations to one such Fourier mode. From this we obtain the following system of algebraic equations:

$$\begin{aligned} \omega \frac{\rho_A}{\rho_0} &= \mathbf{k} \cdot \mathbf{u}_A \\ \omega \mathbf{u}_A &= \gamma \frac{P_0}{\rho_0} \frac{\rho_A}{\rho_0} \mathbf{k}, \end{aligned} \quad (21)$$

which relate the frequency of the mode ω , its wave number \mathbf{k} , the equilibrium values for pressure P_0 and density ρ_0 , and the perturbation amplitudes for density ρ_A and velocity \mathbf{u}_A . Here the acoustic waves are assumed to be an adiabatic process in an ideal gas, so the adiabatic index γ is used in lieu of the energy equation. Manipulating the equations above and using $p\rho^{-\gamma} = \text{constant}$, one can find the explicit relations for the wave amplitude and propagation speed:

$$\begin{aligned} P_A &= c_s^2 \rho_A \\ \mathbf{u}_A &= \frac{\mathbf{k}}{|\mathbf{k}|} c_s \frac{\rho_A}{\rho_0}, \end{aligned} \quad (22)$$

where $c_s \equiv \sqrt{\gamma P_0 / \rho_0}$ is the wave propagation speed, commonly known as the sound speed.

Finally, one can show from the characteristic equation that both the pressure and velocity waves will have two modes traveling in opposite directions and the density wave having a third, stationary mode.

3.6. Performance and scalability

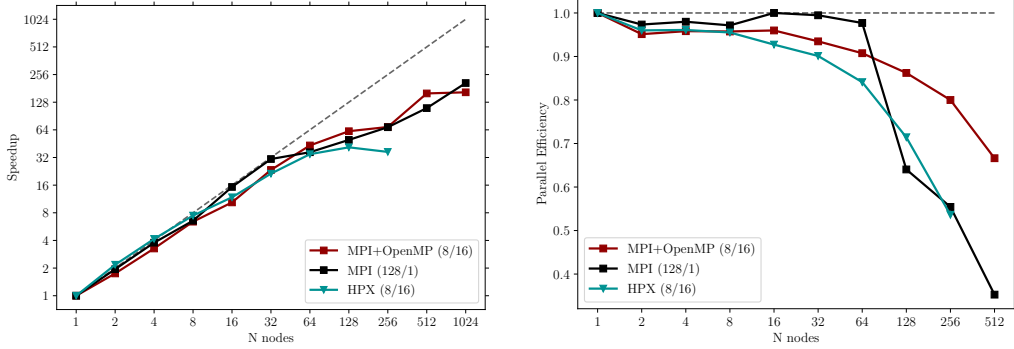


Figure 8: Performance of the 3D radiation benchmark on Chicoma. The notation (128/1) denotes the run configuration as (#processes/#MPI ranks). Left: strong scaling on 1024 nodes shows near-ideal speedup for MPI and MPI+OpenMP (dashed line = ideal linear scaling). Right: weak scaling efficiency, with MPI+OpenMP maintaining 70% on 512 nodes.

We perform our scaling tests on LANL Chicoma supercomputer. Chicoma’s standard partition has 1792 nodes; each node contains two AMD EPYC Rome 64-core CPUs (7H12 @ 2.6 GHz) with 512 GB of memory (16–32 GiB DIMMs). The GPU partition, although not used in the scaling tests presented in Figure 8, consists of 118 nodes equipped with AMD EPYC 7713 processors and NVIDIA A100 GPUs.

The scaling experiments in Figure 8 demonstrate that HARD achieves excellent parallel efficiency on Chicoma. For strong scaling, the 3D radiation benchmark maintains near-ideal speedup up to thousands of cores, confirming that the task-based decomposition in FLECSI combined with Kokkos node-level parallelism enables effective utilization of large CPU partitions. The weak scaling results further show that performance remains consistent as both problem size and node count increase proportionally, indicating that HARD sustains high throughput without degradation when tackling ever-larger workloads.

In addition to these CPU-focused results, we have begun exploring GPU acceleration on Chicoma’s A100 nodes. Preliminary tests show that a single GPU achieves a $7\times$ speedup compared to a CPU node, with performance

reaching 67.6 million cell updates per second. These results highlight the strong potential of HARD on GPU architectures, and ongoing work is focused on scaling across multiple GPUs to fully characterize performance and portability in heterogeneous environments.

Overall, these results validate the design goal of performance portability across both CPU- and GPU-based systems. They demonstrate that HARD can not only exploit existing large-scale clusters efficiently, but also serve as a scalable foundation for even larger simulations expected on forthcoming exascale-class machines.

4. Impact

HARD enables performance-portable simulations that are optimized for modern heterogeneous architectures and extreme-scale parallelism. Our demonstration problems highlight HARD’s ability to accurately and robustly handle a wide variety of physical scenarios, ranging from canonical test problems to application-inspired benchmarks. These position HARD as not only a validation platform for new algorithms, but also a research tool for investigating the fundamental behavior of RHD systems. While additional physics modules may be required to model the full complexity of HEDP phenomena, HARD already serves as a versatile and reliable testbed for exploring a broad class of HEDP problems. Its modularity and scalability position it as a valuable tool for advancing both the development and validation of next-generation HEDP simulation capabilities. Beyond HEDP, HARD’s generality also makes it a valuable tool for astrophysical simulations, laboratory plasma experiments, and other domains where radiation–matter interactions play a central role.

5. Conclusions

We have presented HARD, a performance-portable RHD code built on the FLECSI framework and designed to exploit the capabilities of modern heterogeneous computing architectures. Through a series of benchmark test problems, we have demonstrated the code’s flexibility, accuracy, and usability across a range of relevant scenarios. Looking ahead, we plan to expand HARD by incorporating advanced radiation transport models, including multi-group approaches and higher-order diffusion schemes, thereby enhancing its ability to capture spectral effects and anisotropic transport phenomena. The planned integration of `FleCSolve` will further enable the efficient solution of large-scale implicit radiation systems, a key capability for simulating realistic, high-fidelity HEDP experiments. With these enhancements, HARD is poised to become a robust and accurate tool for tackling

complex RHD problems across diverse disciplines, including HEDP and astrophysics.

Acknowledgements

The HARD project is supported by the Los Alamos National Laboratory (LANL) Advanced Simulation and Computing Program. LANL is operated by Triad National Security, LLC, for the National Nuclear Security Administration of the U.S. Department of Energy (contract no. 89233218CNA000001). This work is authorized for unlimited release under LA-UR-25-27266. The work reported in this paper would not have been possible without close collaborations with the FLECSI and Applications teams.

References

- [1] B. Bergen, I. Demeshko, C. Ferenbaugh, D. Herring, L.-T. Lo, J. Loiseau, N. Ray, A. Reisner, Flecsi 2.0: The flexible computational science infrastructure project, in: European Conference on Parallel Processing, Springer, 2021, pp. 480–495.
- [2] M. Bauer, S. Treichler, E. Slaughter, A. Aiken, Legion: expressing locality and independence with logical regions, in: SC’12: Proceedings of the International Conference on High Performance Computing, Networking, Storage and Analysis, IEEE, 2012, pp. 1–11.
- [3] M. P. I. Forum, Mpi: A message-passing interface standard, Tech. rep., USA (1994).
- [4] H. Kaiser, P. Diehl, A. S. Lemoine, B. A. Lebach, P. Amini, A. Berge, J. Biddiscombe, S. R. Brandt, N. Gupta, T. Heller, K. Huck, Z. Khatami, A. Kheirhahan, A. Reverdell, S. Shirzad, M. Simberg, B. Wagle, W. Wei, T. Zhang, Hpx - the c++ standard library for parallelism and concurrency, *Journal of Open Source Software* 5 (53) (2020) 2352. doi:10.21105/joss.02352.
URL <https://doi.org/10.21105/joss.02352>
- [5] H. C. Edwards, C. R. Trott, D. Sunderland, Kokkos: enabling manycore performance portability through polymorphic memory access patterns, *Journal of Parallel and Distributed Computing* 74 (12) (2014) 3202–3216.

- [6] N. J. Turner, J. M. Stone, A module for radiation hydrodynamic calculations with zeus-2d using flux-limited diffusion, *The Astrophysical Journal Supplement Series* 135 (1) (2001) 95. doi:10.1086/321779. URL <https://dx.doi.org/10.1086/321779>
- [7] B. van der Holst, G. Toth, I. V. Sokolov, K. G. Powell, J. P. Holloway, E. S. Myra, Q. Stout, M. L. Adams, J. E. Morel, R. P. Drake, Crash: A Block-Adaptive-Mesh Code for Radiative Shock Hydrodynamics - Implementation and Verification, *Astrophys. J. Suppl.* 194 (2011) 23. arXiv:1101.3758, doi:10.1088/0067-0049/194/2/23.
- [8] W. Zhang, L. Howell, A. Almgren, A. Burrows, J. Bell, CASTRO: A New Compressible Astrophysical Solver. II. Gray Radiation Hydrodynamics, *Astrophys. J. Suppl.* 196 (2011) 20. arXiv:1105.2466, doi:10.1088/0067-0049/196/2/20.
- [9] Y.-F. Jiang, Multigroup Radiation Magnetohydrodynamics Based on Discrete Ordinates including Compton Scattering, *Astrophys. J. Suppl.* 263 (1) (2022) 4. arXiv:2209.06240, doi:10.3847/1538-4365/ac9231.
- [10] N. Moens, J. O. Sundqvist, I. El Mellah, L. Poniowski, J. Teunissen, R. Keppens, Radiation-hydrodynamics with MPI-AMRVAC . Flux-limited diffusion, *A&A* 657 (2022) A81. arXiv:2104.03968, doi:10.1051/0004-6361/202141023.
- [11] B. D. Wibking, M. R. Krumholz, QUOKKA: a code for two-moment AMR radiation hydrodynamics on GPUs, *MNRAS* 512 (1) (2022) 1430–1449. arXiv:2110.01792, doi:10.1093/mnras/stac439.
- [12] T. Gamblin, M. LeGendre, M. R. Collette, G. L. Lee, A. Moody, B. R. de Supinski, S. Futral, The Spack Package Manager: Bringing Order to HPC Software Chaos, *Supercomputing 2015 (SC'15)*, Austin, Texas, USA, 2015, ILNL-CONF-669890. doi:10.1145/2807591.2807623. URL <https://github.com/spack/spack>
- [13] U. Ayachit, *The ParaView Guide: A Parallel Visualization Application*, Kitware, Inc., Clifton Park, NY, USA, 2015. URL <https://www.paraview.org/paraview-guide/>
- [14] H. Childs, E. Brugger, B. Whitlock, J. Meredith, S. Ahern, D. Pugmire, K. Biagas, M. Miller, C. Harrison, G. H. Weber, H. Krishnan, T. Fogal, A. Sanderson, C. Garth, E. W. Bethel, D. Camp, O. Rübel, M. Durrant, J. M. Favre, P. Navrátil, VisIt: An End-User Tool For Visualizing

- and Analyzing Very Large Data, in: High Performance Visualization—Enabling Extreme-Scale Scientific Insight, 2012, pp. 357–372.
- [15] D. Mihalas, B. W. Mihalas, Foundations of radiation hydrodynamics, Dover Publications, INC., 1984.
 - [16] singularity-eos, <https://github.com/lanl/singularity-eos> (aug 25 2025). URL <https://github.com/lanl/singularity-eos>
 - [17] C. D. Levermore, G. C. Pomraning, A flux-limited diffusion theory, Astrophysical Journal 248 (1981) 321–334. doi:10.1086/159157.
 - [18] R. Borges, M. Carmona, B. Costa, W. S. Don, An improved weighted essentially non-oscillatory scheme for hyperbolic conservation laws, Journal of Computational Physics 227 (6) (2008) 3191–3211. doi:10.1016/j.jcp.2007.11.038.
 - [19] A. Harten, P. D. Lax, B. v. Leer, On upstream differencing and godunov-type schemes for hyperbolic conservation laws, SIAM Review 25 (1) (1983) 35–61. doi:10.1137/1025002. URL <https://doi.org/10.1137/1025002>
 - [20] V. Rusanov, The calculation of the interaction of non-stationary shock waves and obstacles, USSR Computational Mathematics and Mathematical Physics 1 (2) (1962) 304–320. doi:[https://doi.org/10.1016/0041-5553\(62\)90062-9](https://doi.org/10.1016/0041-5553(62)90062-9). URL <https://www.sciencedirect.com/science/article/pii/0041555362900629>
 - [21] W. L. Briggs, V. E. Henson, S. F. McCormick, A Multigrid Tutorial, Second Edition, 2nd Edition, Society for Industrial and Applied Mathematics, 2000. arXiv:<https://epubs.siam.org/doi/pdf/10.1137/1.9780898719505>, doi:10.1137/1.9780898719505. URL <https://epubs.siam.org/doi/abs/10.1137/1.9780898719505>
 - [22] U. Trottenberg, C. W. Oosterlee, S. Anton, Multigrid, Elsevier, 2000.
 - [23] A. Reisner, C. Mauney, flecsolve (03 2025). doi:10.11578/dc.20250418.2. URL <https://www.osti.gov/biblio/code-154403>
 - [24] N. Roth, D. Kasen, Monte carlo radiation-hydrodynamics with implicit methods, The Astrophysical Journal Supplement Series 217 (1) (2015) 9. doi:10.1088/0067-0049/217/1/9. URL <https://dx.doi.org/10.1088/0067-0049/217/1/9>

- [25] ASC, xrage user manual, Tech. rep., LANL (2023).
- [26] S. Chandrasekhar, Hydrodynamic and hydromagnetic stability, 1961.
- [27] M. Shadmehri, Z. Enayati, M. Khajavi, Magnetized kelvin-helmholtz instability in the presence of a radiation field, *Astrophysics and Space Science* 341 (2) (2012) 369–374. doi:10.1007/s10509-012-1096-4. URL <https://doi.org/10.1007/s10509-012-1096-4>
- [28] H. Peng, F. Yu, Y. Huliuta, L. Wei, Z.-X. Wang, Y. Liu, Effect of Transverse Magnetic Field on Kelvin–Helmholtz Instability in the Presence of a Radiation Field, *Astrophysical Journal* 970 (1) (2024) 3. doi:10.3847/1538-4357/ad5312.